OXFORD

Carcinogenesis, 2015, Vol. 36, No. 11, 1263–1274

doi:10.1093/carcin/bgv124
Advance Access publication September 8, 2015
Original Manuscript

ORIGINAL MANUSCRIPT

Autophagy-mediated degradation of nuclear envelope proteins during oncogene-induced senescence

Christelle Lenain[1], Olga Gusyatiner[1,3], Sirith Douma[1], Bram van den Broek[2] and Daniel S. Peeper[1,*]

[1]Division of Molecular Oncology and [2]Division of Cell Biology I, The Netherlands Cancer Institute, 1066 CX Amsterdam, The Netherlands [3]Present address: Laboratory of Brain Tumor Biology and Genetics, Department of Neurosurgery, Lausanne University Hospital (CHUV), 1011 Lausanne, Switzerland

*To whom correspondence should be addressed. Tel: +31 512 2099; Fax: +31 20 669 1383; Email: d.peeper@nki.nl

Abstract

Cellular senescence is a largely irreversible form of cell cycle arrest triggered by various types of damage and stress, including oncogene expression (termed oncogene-induced senescence or OIS). We and others have previously demonstrated that OIS occurs in human benign lesions, acting as a potent tumor suppressor mechanism. Numerous phenotypic changes occur during OIS, both in the cytoplasm and in the nucleus. These include the activation of autophagy, a catabolic process operating in the cytoplasm and downregulation of lamin B1, a component of the nuclear lamina. However, it is unknown whether these changes relate to each other. We discovered that cells entering $BRAF^{V600E}$- or $H\text{-}RAS^{G12V}$-induced senescence downregulate not only lamin B1 but also lamin A, as well as several other nuclear envelope (NE) proteins, resulting in an altered NE morphology. Depletion of *LMNB1* or *LMNA/C* was sufficient to recapitulate some OIS features, including cell cycle exit and downregulation of NE proteins. We further found that the global loss of NE proteins is a consequence of their degradation by the autophagy machinery, which occurs concomitantly with autophagy induction and increased lysosomal content and activity. Our study therefore reveals a previously unknown connection between autophagy and the disruption of NE integrity during OIS.

Introduction

Cellular senescence is a virtually irreversible form of cell cycle arrest that occurs in response to diverse stress signals, including telomere shortening and oncogene activation (oncogene-induced senescence or OIS) (1). Several studies have demonstrated that this phenomenon, which was initially identified and characterized *in vitro*, acts as a robust tumor suppressor mechanism *in vivo* (2–5). For instance, our laboratory demonstrated key characteristics of OIS in a benign human lesion, the melanocytic nevus, which led us and others to propose that OIS prevents progression from nevi to malignant melanoma (2,6).

Given the pivotal role of senescence in the pathogenesis of human cancer, there is a crucial need to dissect the mechanisms underlying this failsafe program. Numerous phenotypic changes have been described as hallmarks of senescence—including OIS—with several of them actively contributing to the process. Some changes occur in the cytoplasm, such as altered metabolic activity (7,8) and increased autophagy (9,10), while others affect the nucleus, like the accumulation of senescence-associated heterochromatic foci (SAHF) (11,12). We still have an incomplete understanding of the relative importance of these cytoplasmic and nuclear events, and whether they relate to each other is totally unknown.

The nuclear envelope (NE) encloses the nucleus in eukaryotic cells. It consists of two membranes, its associated inner nuclear membrane (INM) proteins and the nuclear lamina (NL). The latter is a filamentous network lining the INM and composed of A-type and B-type lamins (13). The NL plays an important role in the three-dimensional organization of the nucleus by stabilizing the NE (14) and by interacting with specific chromosomal regions called lamina-associated domains (15). Through this

Received: January 5, 2015; **Revised:** July 9, 2015; **Accepted:** July 16, 2015

Abbreviations

INM	inner nuclear membrane
LBR	lamin B receptor
NE	nuclear envelope
NL	nuclear lamina
OIS	oncogene-induced senescence
PEI	polyethylenimine
PBS	phosphate-buffered saline

architectural function the NL contributes to nuclear processes that are essential for cellular physiology, such as regulation of gene expression and DNA replication (16,17).

Several lines of evidence have implicated lamins and NE alterations in cellular senescence. First, mutations in lamin A cause premature aging syndromes. This is the case in Hutchinson–Gilford progeria syndrome, a condition caused by a mutation that creates an aberrant splice variant of lamin A called progerin (18,19). Cells from Hutchinson–Gilford progeria syndrome patients present nuclear malformations and senesce prematurely *in vitro* (20). Along these lines, replicatively senescent cells and ageing tissues from healthy individuals also accumulate progerin (21). More recent data has pointed to an involvement of downregulation of lamin B1 and less consistently of lamin A in several types of senescence, including OIS (22–26). So far, the functional significance of these deregulations in OIS has remained unclear.

Here, we show that the expression of lamins and several INM proteins is decreased during OIS, which is associated with disruption of NE morphology. We further demonstrate that NE protein downregulation is caused by autophagy, revealing a relationship between enhanced cytoplasmic catabolic processes and disruption of NE integrity during OIS.

Materials and methods

Plasmids and virus production

The retroviral vectors pBabe-puro and pBabe-puro-BRAF^{V600E} or H-RAS^{G12V} were used to overexpress the oncogene BRAF^{V600E} or H-RAS^{G12V} in Tig3ET and IMR90ET cells. The lentiviral vectors HIV-CS-CG and HIV-CS_CG-BRAF^{V600E} were used to transduce melanocytes and ATG5 shRNA-expressing Tig3ET cells. The following lentiviral shRNA vectors were obtained from the human TRC shRNA library:
sh-LMNB1 #71: TRCN0000029271_ GCATGAGAATTGAGAGCCTTT
sh-LMNB1 #72: TRCN0000029272_ GCTCAAAGAAGTACAGTCTTT
sh-LMNA/C #35: TRCN0000061835_ GAAGCAACTTCAGGATGAGAT
sh-LMNA/C #37: TRCN0000061837_ GCCGTGCTTCCTCTCACTCAT
sh-ATG5 #394: TRCN0000330394_ CCTGAACAGAATCATCCTTAAC
sh-ATG5 #963: TRCN0000151963_ CCTGAACAGAATCATCCTTAA
Retroviruses were produced in the Phoenix packaging cell line using polyethylenimine (PEI) transfection method. One day prior transfection, 2.5–2.8 × 10^6 cells per 10 cm dish were seeded. Twenty four hours later the cells were transfected with a mix of 400 µl of Optimem containing 1.25 µg/ml of an EGFP-encoding plasmid (used as a transfection efficiency marker), 25 µg of expression plasmid and PEI used at 1:2 ratio [(DNA (µg)/PEI (µl)] per 10 cm dish. Culture medium was refreshed with fresh Dulbecco's modified Eagle's medium the next morning. The first supernatant was collected 48 h after transfection and then two more times at 12 h intervals. Production of lentiviruses was performed in HEK293T packaging cell line also using PEI transfection. One day prior to transfection HEK293T cells were seeded at 3.4 × 10^6 cells/10 cm dish. Twenty four hours later, the cells were transfected with 8 µg of expression plasmid and 3 µg of each of the packaging plasmids (pRSVrev, pHCMV-G, pMDLgIpRRE) using the same PEI transfection procedure as for the retrovirus production except that PEI was used at a 1:3 ratio. Supernatant was first collected 48 h post-transfection and then two more times every 12 h.

Cell lines

The Tig3 fibroblast cell line was provided by Kumiko Anno (Hiroshima University, Japan) in 1999. The IMR90 cell line was purchased from ATCC. We introduced into Tig3 and IMR90 the ecotropic receptor and hTERT to prevent replicative senescence (Tig3ET and IMR90ET). We also used Tig3ET derivative expressing SV40 small t (st). These HDF lines were propagated in Dulbecco's modified Eagle's medium, supplemented with 9% fetal bovine serum. The fibroblast cell-line expressing a tet-off driven GFP progerin was provided by Tom Mistelli (National Cancer Institute, NIH, Bethesda) and maintained in modified Eagle's medium, supplemented with 15% fetal calf serum and doxycyclin at 1 g/ml. Melanocytes were generated and propagated as described in (2). OIS was induced in Tig3ET cells by transduction with retroviruses encoding BRAF^{V600E}, or H-RAS^{G12V} as described in (2). OIS was induced in human melanocytes by transduction with lentiviruses encoding BRAF^{V600E} as described in (2). Tig3 cells were used to generate replicative senescent cells by prolonged passaging. Early passage cells were harvested at PD 43–44; late passage cells were harvested at PD 72–73. Authentication of the Tig3ET and IMR90ET cell line was performed by STR profiling using the Power Plex 16 HS System (Promega). The last tests were performed in September 2014. No authentication was performed for the fibroblast cell-line expressing a tet-off driven GFP progerin or for the melanocyte cell line generated in our lab.

Cell proliferation assays

Six days or 9 days after infection with BRAF^{V600E}- or H-RAS^{G12V}-encoding retroviruses, cells were seeded for BrdU, cell proliferation and senescence-associated β-galactosidase assays. For BrdU incorporation analysis, cells were seeded in 6 cm dishes so that they reach subconfluency at the time of harvesting; the next day they were incubated with BrdU (Roche) at a final concentration of 10µM. For proliferation assays, cells were seeded into a six-well plate at 4 × 10^4 cells/well and fixed and stained 11–15 days after infection with crystal violet. For senescence-associated β-galactosidase assays, cells were seeded in eight-well chambers so that they reach subconfluency at the time of fixation and stained using the Senescence β-galactosidase Staining kit from Cell signaling following the manufacturer's instructions. Images were acquired on a Zeiss Axiovert S100 inverted microscope coupled with a Zeiss AxioCam color camera (Axiocam HRc).

Western blotting

Cells were lysed in RIPA buffer (50mM Tris–HCl Buffer pH 8.0, 150mM NaCl, 1% NP40, 5% sodium deoxycholate, 0.1% SDS) supplemented with cocktails of phosphatase and protease inhibitors. Samples corresponding to 20 µg of protein were separated by SDS_PAGE (reduced NuPAGE 4–12%, BisTris gels Life technologies, MES running buffer, Life Technologies) and transferred to nitrocellulose membranes (Millipore). The membrane was blocked with 5% non-fat milk in phosphate-buffered saline (PBS)-T buffer (1× PBS containing 0.02% tween). Antibodies used were against BRAF (sc-5284), Ras (BD Transduction Laboratories, 610001), p16 (sc-56330), p15 (sc-612), p21 (sc-397), HSP90 (sc-7947), CDK4 (sc-260), p16INK4A (JC8; MS-889, Neomarkers), lamin B1 (ab16048), lamin B2 (sc-56146), lamin A/C (sc-6215), emerin (10351-1-AP, Proteintech Group), LBR (ab122919), MAN1 (ab114031), SUN1 (ab74758), ubiquitin (sc-8017), LC3 (231-100, Nanotools), cathepsin C (LS-C137510, Lifespan Biosciences), cathepsin D (LS-B2931, Lifespan Biosciences), cathepsin L (ab6314), PRPC (15995-1-AP, Proteintech Group), ATG5 (GTX48583, GeneTex).

Drug treatment

Six days after infection, cells were seeded on 10 cm dishes. The next day cells were treated with 100 nM bafilomycin A1 (Santa Cruz, sc-20155A) for 8 h, 50 or 100 µM chloroquine for 6 h (Sigma, C06622), or 2.5 mM epoxomicin (Boston Biochem I-110) for 3.5 h. Etoposide was used at a 10 µM concentration for 13 days.

Immunofluorescence microscopy

Six days after infection, cells were seeded on eight-well chambers, so that they reach subconfluency at the time of fixation. The next day, cells were fixed in 2% formaldehyde/PBS for 10 min, washed twice with PBS and permeabilized with 0.5% Triton X-100/PBS for 10 min. After a blocking step with 5% goat or calf serum in PBS-T (PBS containing 0.2% tween) for

30 min, cells were incubated for 1 h at room temperature with the primary antibodies in blocking solution. The cells were then washed three times in PBS-T and incubated with fluorophore-conjugated secondary antibodies for 1 h at room temperature. After three washes, the cells were stained with 4′,6-diamidino-2-phenylindole at 1:5000 in PBS. Then the slides were dried and mounted with vectashield. The antibodies used were anti lamin B1 (ab16048), rabbit anti-emerin (Proteintech Group 10351-1-AP), anti-progerin (Ab 66587), anti LAMP2 (sc-1882). The following secondary antibodies were used: Alexa Fluor-488 or -568 goat anti-rabbit, Alexa Fluor-488 or -568 goat anti-mouse, Alexa Fluor-488 donkey anti-goat (Invitrogen). Image acquisition was performed on a Leica TCS SP5 confocal laser-scanning microscope using 63×/1.4NA oil immersion objective. Images were acquired as Z-stacks using sequential scanning mode. Lamin B1 fluorescence intensity was quantified using Fiji software. Lamin B1 fluorescence intensity was quantified semi-automatically using an in-house developed macro in ImageJ. Nuclei were segmented by thresholding a filtered and background-subtracted maximum intensity projected image, followed by a watershed operation to separate touching nuclei. Segmented regions of interest were visually inspected and were merged or deleted where necessary. Intranuclear Lamin B1 intensity was measured in slightly eroded regions of interest (3 pixels) to exclude the nuclear perimeter, and was calculated by summing the background-exceeding intensity of pixels whose gray level was larger than the intranuclear background staining by at least three times the standard deviation of the background.

Transmission electron microscopy

Cells were fixed in 2% paraformaldehyde and 0.2% glutaraldehyde in 0.1 M PHEM (240 mM PIPES, 100 mM HEPES, 8 mM, MgCL2, 40mM EGTA, pH6.9) and processed for ultrathin cryosectioning. The cryosections were embedded in uranylacetate and methylcellulose and imaged with a Philips CM 10 electron microscope (FEI Eindhoven, The Netherlands).

RNA isolation and real-time quantitative PCR

Total RNA was isolated using TRIzol (Invitrogen). Total RNA was treated with DNAse I. Reverse transcription was performed with Superscript II first strand kit (Invitrogen). QRT-PCR was performed with the SYBR Green PCR Master Mix (Applied Biosystems) on an ABI PRISM 7700 Sequence Detection System. Primer sequences are described in Supplementary Table 1, available at *Carcinogenesis* Online. Fold change values were calculated using the DDCt method. Briefly, RPL13 was used as 'normalizer' gene to calculate the DCt value. Next, the DDCt value was calculated between the 'control' group and the 'experimental' group. Lastly, the fold change was calculated using 2(–DDCt). Biological replicates were grouped in the calculation of the fold change values.

Results

NE proteins are downregulated during OIS

We first investigated whether lamin levels are altered during OIS. For this, we used human diploid fibroblast (Tig3ET) induced to senesce by ectopic expression of $BRAF^{V600E}$ or $H\text{-}RAS^{G12V}$. As expected, expression of these two oncogenes resulted in senescence as manifested by a decrease in BrdU incorporation, an increase in senescence-associated-β-galactosidase (SA-β-GAL) activity and an induction of the CDK inhibitors $p16^{INK4A}$, $p15^{INK4B}$ or $p21^{Cip1}$ (Supplementary Figure 1A, B and C, available at *Carcinogenesis* Online). Western blot analysis showed that OIS was associated with a downregulation of lamin B1, lamin B2 and lamin A (Figure 1A and B). This loss of lamin expression occurred both upon $BRAF^{V600E}$ and $H\text{-}RAS^{G12V}$-induced senescence, whereas in cells rendered quiescent by 7 days of serum starvation all lamins remained unaltered, indicating that this downregulation is not a consequence of cell cycle exit (Figure 1A and B).

To confirm the western blot data, we performed immunofluorescence staining for lamin B1 (Figure 1C). Quantification of the lamin B1 mean fluorescence intensity per nucleus confirmed a significant downregulation specifically in OIS cells (Figure 1D). Remarkably $BRAF^{V600E}$-senescent cells also showed a decline in emerin and other INM proteins, indicative of an overall loss of NE protein expression during OIS (Figure 1E and F).

NE proteins were also downregulated upon $BRAF^{V600E}$-induced senescence in hTERT-immortalized IMR90ET fibroblasts, as well as in human skin melanocytes, (Figure 1G and H, and Supplementary 1D, available at *Carcinogenesis* Online), indicating that this phenotype is not unique to human diploid fibroblasts.

NE protein downregulation is a common feature of senescence

We also examined NE protein levels in Tig3 cells induced to senesce by extensive passaging or exposure to the DNA damage-inducing agent etoposide. Both conditions triggered a robust senescence phenotype, as demonstrated by decreased BrdU incorporation, induction of SA-β-GAL activity (Supplementary Figure 2A and C, available at *Carcinogenesis* Online) and elevated levels of $p21^{Cip1}$ and $p16^{INK4A}$ (Supplementary Figure 2B and 2D, available at *Carcinogenesis* Online). Both types of senescence were associated with declines of lamin A and B1, as well the INM proteins lamin B receptor (LBR) and MAN1 (Figure 2A–D). Loss of lamin B1 expression was confirmed by immunofluorescence microcopy (Figure 2E and F). In both senescence settings, emerin levels remained unaffected, whereas expression of SUN1 was increased (Figure 2C and D). It remains unknown why the pattern of regulation of INM proteins differs in cells experiencing OIS versus replicative or DNA damage-induced senescence. Nonetheless, these results indicate that loss of expression of lamin B1, lamin A, LBR and MAN1 is a common characteristic of cellular senescence.

OIS cells display disrupted NE structure

The loss of NE protein expression could conceivably result in alteration of the NE structure, which we investigated by immunofluorescent confocal microscopy. These experiments revealed that a significant proportion of OIS cells had an aberrant pattern of residual intranuclear lamin B1 staining, which gave them the appearance of a shriveled nucleus (Figure 3A). This was also manifested by a significant increase in the lamin B1 fluorescence intensity in the nucleus interior (Figure 3B). Further, electron microscopy analysis revealed the presence of NE invaginations inside the nucleus, indicating that not only the NL but also the entire NE structure is disrupted in OIS (Figure 3C). Moreover, Tig3 cells induced to senesce by extensive passaging undergo similar alterations of nuclear morphology (Figure 3D and E). Thus, altered NE structure appears to be a conserved phenotype across diverse types of senescence.

Depletion of lamin B1 and A/C partially recapitulates the senescence phenotype and NE defects seen in OIS cells

We next asked whether lamin B1 or A loss was sufficient to induce NE alterations and senescence. For this, we investigated the effect of *LMNB1* and *A/C* depletion using two independent non-overlapping shRNAs targeting these two genes in Tig3ET cells. Western blot analysis confirmed that each of the two *LMNB1* or *LMNA/C* shRNAs promoted efficient knockdown of their respective target proteins (Figure 4A). In agreement with previous reports (22,24,27), *LMNB1* and *LMNA/C* depletion resulted in a robust proliferative arrest (Figure 4B). The *LMNB1* and *LMNA/C* shRNAs also induced an increase in SA-β-GAL activity, with the *LMNB1* shRNAs having a more pronounced effect (Figure 4C). For *LMNB1* depletion, we also observed the

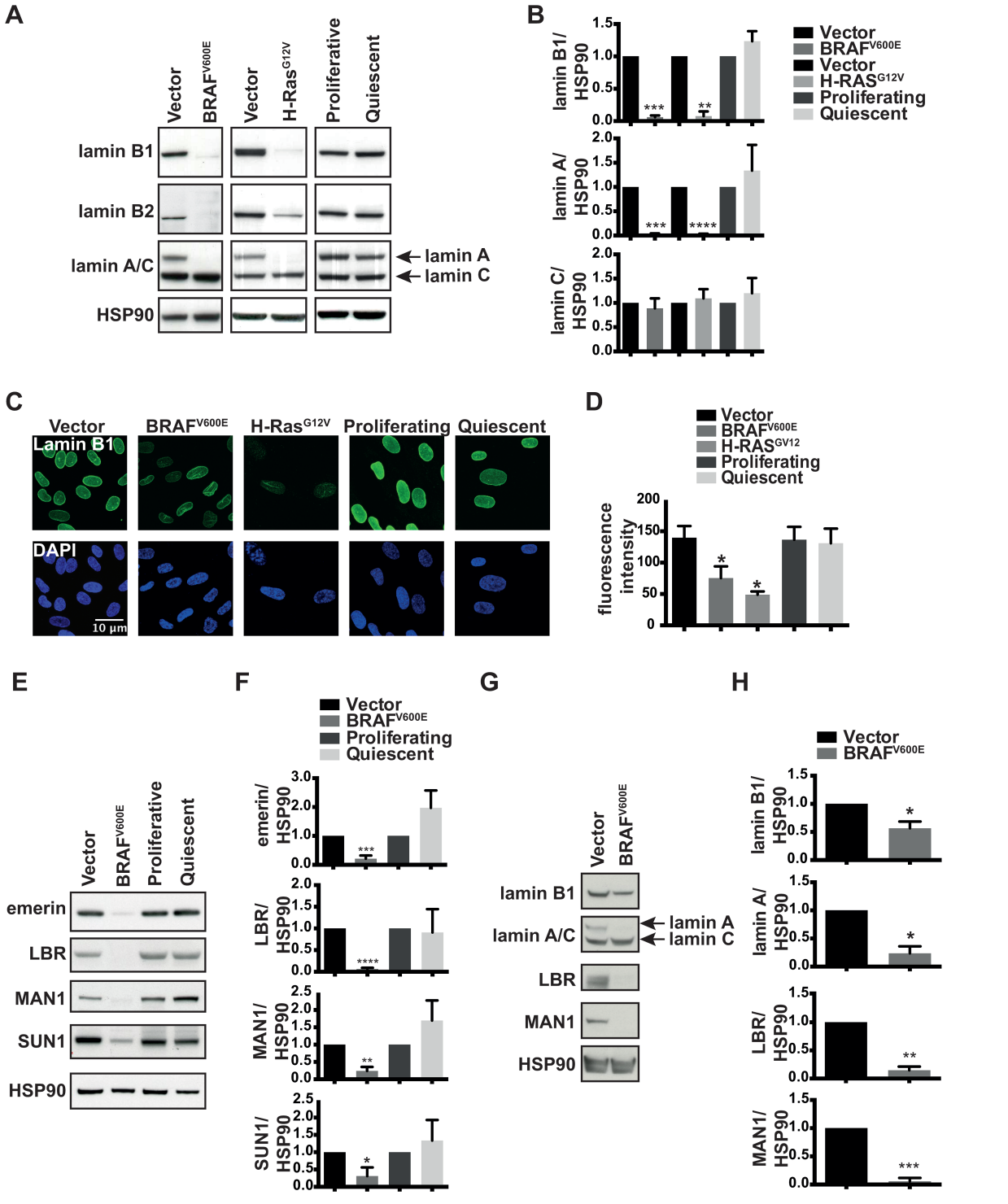

Figure 1. Lamins and INM proteins are downregulated during OIS. (**A**) Immunoblotting was performed with the indicated antibodies on whole-cell lysates from Tig3ET BRAF^{V600E}- or H-RAS^{G12V} senescent cells harvested at day 7 or day 10 after transduction respectively and from cells made quiescent by serum starvation for 7 days. (**B**) Quantification of the WB signal from (A). Lamin levels were normalized to HSP90. Data are presented as mean and standard deviation of three independent experiments. Asterisks indicate $P < 0.01$ (**), $P < 0.001$ (***) and $P < 0.0001$ (****), based on a two-tailed paired *t* test. (**C**) Immunofluorescence microscopy showing decreased lamin B1 immunofluorescence in BRAF^{V600E}- and H-RAS^{G12V} -senescent Tig3ET cells. Cells were fixed at day 7 (BRAF^{V600E}) or 10 (H-RAS^{G12V}) after transduction. DAPI was used for DNA staining. (**D**) Quantification of the mean lamin B1 fluorescence intensities from (B). Data are presented as mean and standard deviation of at least three independent experiments. Quantification was performed on at least 150 nuclei. Asterisk: $P < 0.05$ based on a two-tailed paired *t*-test. (**E**) Immunoblotting of lysates from Tig3ET fibroblasts 7 days after transduction with BRAF^{V600E} or Tig3ET fibroblasts made quiescent by serum starvation for 7 days with antibodies against the indicated INM proteins. (**F**) Quantification of the WB signal from (E). Protein levels were normalized to HSP90. Data are presented as mean and standard deviation of three independent experiments. Asterisks indicate $P < 0.05$(*), $P < 0.01$(**), $P < 0.001$ (***) and $P < 0.0001$ (****), based on a two-tailed paired *t* test. (**G**) Immunoblotting analysis of NE protein expression in human melanocytes 13 days after transduction with BRAF^{V600E} - encoding lentivirus. (**H**) Quantification of the WB signal from (G). Protein level were normalized to HSP90. Data are presented as mean and standard deviation of two independent experiments. Asterisks indicate $P < 0.05$ (*), $P < 0.01$ (**) and $P < 0.001$ (***), based on a two-tailed paired *t* test.

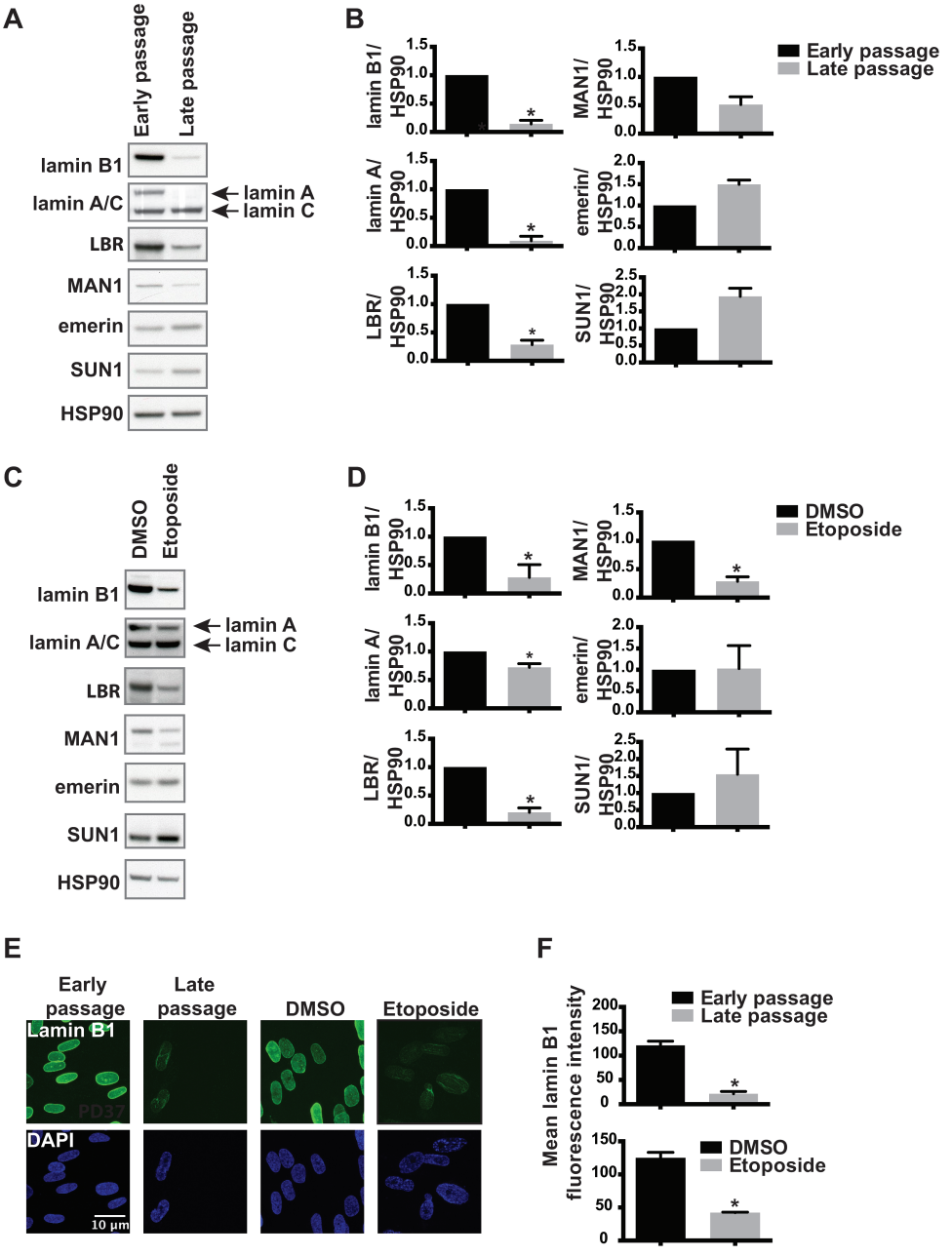

Figure 2. Downregulation of NE proteins in other types of senescence. (**A**) Immunoblotting for lamins and NE proteins of lysates from Tig3 fibroblasts after induction of replicative senescence upon extended in vitro passaging. (**B**) Quantification of the WB signal from (A). Protein levels were normalized to HSP90. Data are presented as mean and standard deviation of two independent experiments. Asterisk indicates $P < 0.05$(*) based on a two-tailed paired *t* test. (**C**) Immunoblotting for lamins and NE proteins of lysates from Tig3ET fibroblasts after treatment with the DNA damaging agent etopside (10 M for 13 days). (**D**) Quantification of the WB signal from (C). Protein levels were normalized to HSP90. Data are presented as mean and standard deviation of two independent experiments. Asterisk indicates $P < 0.05$(*) based on a two-tailed paired *t* test. (**E**) Immunofluorescence confocal microscopy showing decreased lamin B1 signal in Tig3 cells undergoing replicative senescence or DNA damaged-induced senescence. (**F**) Quantification of the mean lamin B1 fluorescence intensities from (E). Data are presented as mean and standard error of the mean of two independent experiments ($n = 200$). Asterisk: $P < 0.05$ based on a two-tailed paired *t*-test.

formation of SAHF (Figure 4D), another hallmark of senescent cells (11). Depletion of *LMNB1* or *LMNA/C* did not induce other established senescence biomarkers, including the induction of the tumor suppressors p16 and p21 (Supplementary Figure 4A and 4B, available at *Carcinogenesis* Online) and the OIS-associated inflammatory factors *IL6* and *C/EBP* (Supplementary Figure 4C, available at *Carcinogenesis* Online). The latter was only seen for one shRNA targeting *LMNA/C* which we therefore attribute to an off-target effect. We conclude that depletion of *LMNB1* or *LMNA/C* triggers cells to exit the cell cycle with some features of senescence.

We then investigated whether depletion of lamin B1 or A/C results in general downregulation of NE proteins. Suppression of Lamin B1 led to a mild decrease in lamin A. Conversely, lamin A/C depletion led to a reduction of lamin B1 (Figure 4A). This reciprocal regulation was not explained by targeting of homologous regions of *LMNA* and *LMNB1* by the different shRNAs. *LMNB1* depleted cells, also displayed downregulation of LBR and MAN1

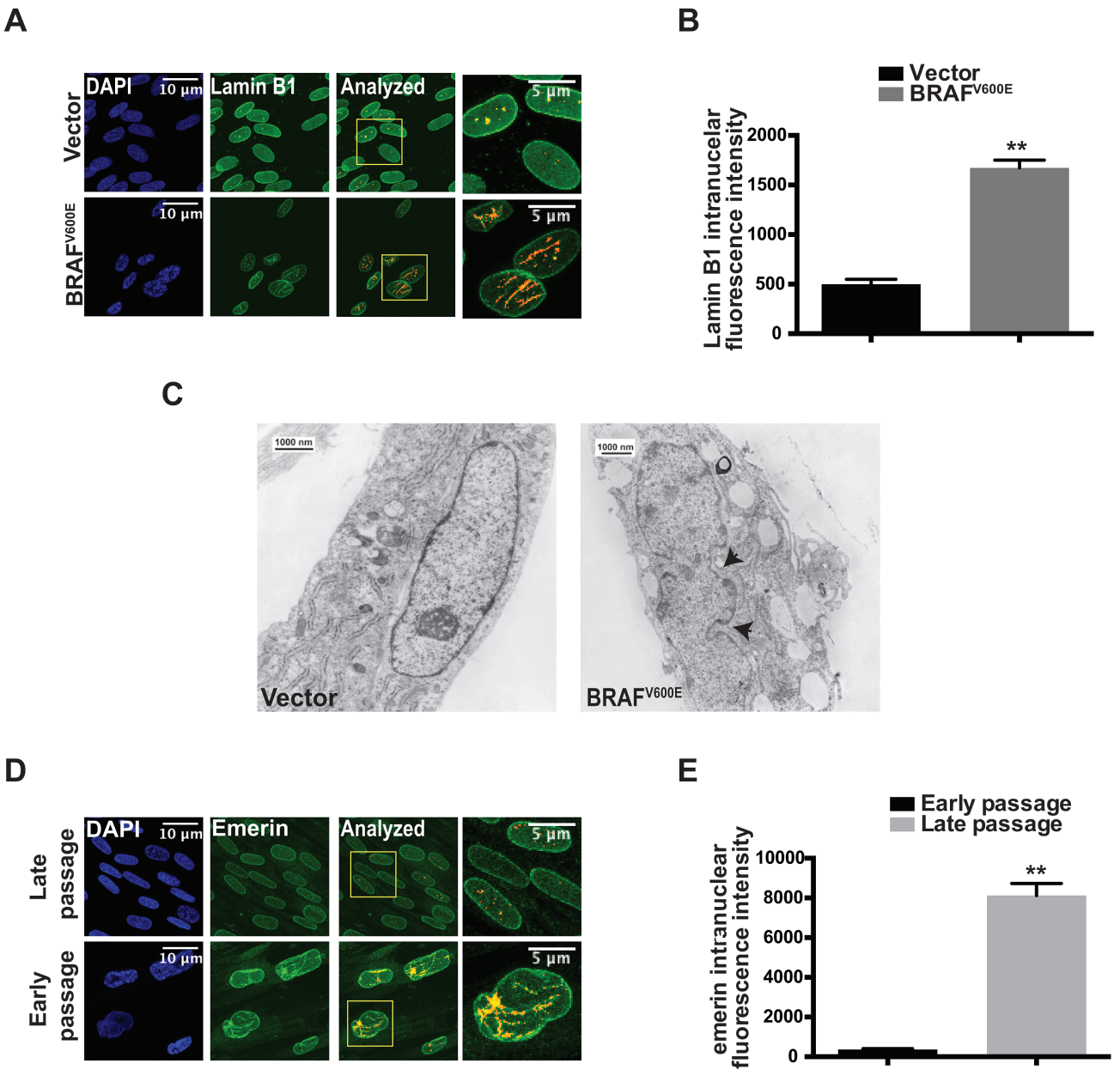

Figure 3. Senescent cells display aberrant nuclear morphology. (**A**) Immunofluorescence microscopy showing aberrant intranuclear accumulation of lamin B1 in $BRAF^{V600E}$-senescent Tig3ET cells. DAPI was used for DNA staining. (**B**) Quantification of lamin B1 fluorescence intensity inside the nucleus. Data are presented as mean and standard error of the mean of at least three independent experiments. Quantification was performed on at least 150 nuclei. Asterisk: $P < 0.05$ based on a two-tailed paired *t*-test. (**C**) Electron microscopy analysis of vector control or $BRAF^{V600E}$-senescent Tig3ET cells showing NE malformations in $BRAF^{V600E}$-senescent cells. Arrowheads indicate NE invaginations. (**D**) Immunofluorescence microscopy showing aberrant intranuclear accumulation of emerin in replicatively senescent Tig3 cells. DAPI was used for DNA staining. (**E**) Quantification of emerin fluorescence intensity inside the nucleus. Data are presented as mean and standard deviation of at least three independent experiments. Quantification was performed on at least 200 nuclei. Asterisks: $P < 0.01$ based on a two-tailed paired *t*-test.

(although the latter was seen for only one shRNA). Silencing of *LMNA/C* by the two shRNAs resulted in MAN1 repression. On the other hand, knockdown of neither LMNB1 nor LMNA/C affected the levels of emerin or SUN1 (Figure 4E). Therefore, individual downregulation of lamin B1 or lamin A/C is sufficient to trigger a partial loss of NE protein expression.

To determine the consequences of *LMNB1* and *LMNA/C* knockdown on nuclear architecture, we performed immunofluorescence microscopy for emerin. This analysis revealed that the effect of *LMNB1* or *LMNA/C* knockdown on nuclear morphology was distinct from that seen during OIS. Indeed, a small but significant fraction of *LMNB1* knockdown cells displayed nuclear blebbing (Figure 4F), a phenotype that was absent in *LMNA* knockdown and OIS cells. Of note, nuclear blebbing have also been observed after depletion of lamin B1 in HeLa cells (28). In conclusion, *LMNB1* and *LMNA* knockdown partially recapitulates the senescence phenotype and the NE defects associated with OIS.

Macroautophagy mediates NE protein proteolysis during OIS

We next sought to determine the mechanisms responsible for NE protein downregulation during OIS. Lamin B1 was previously

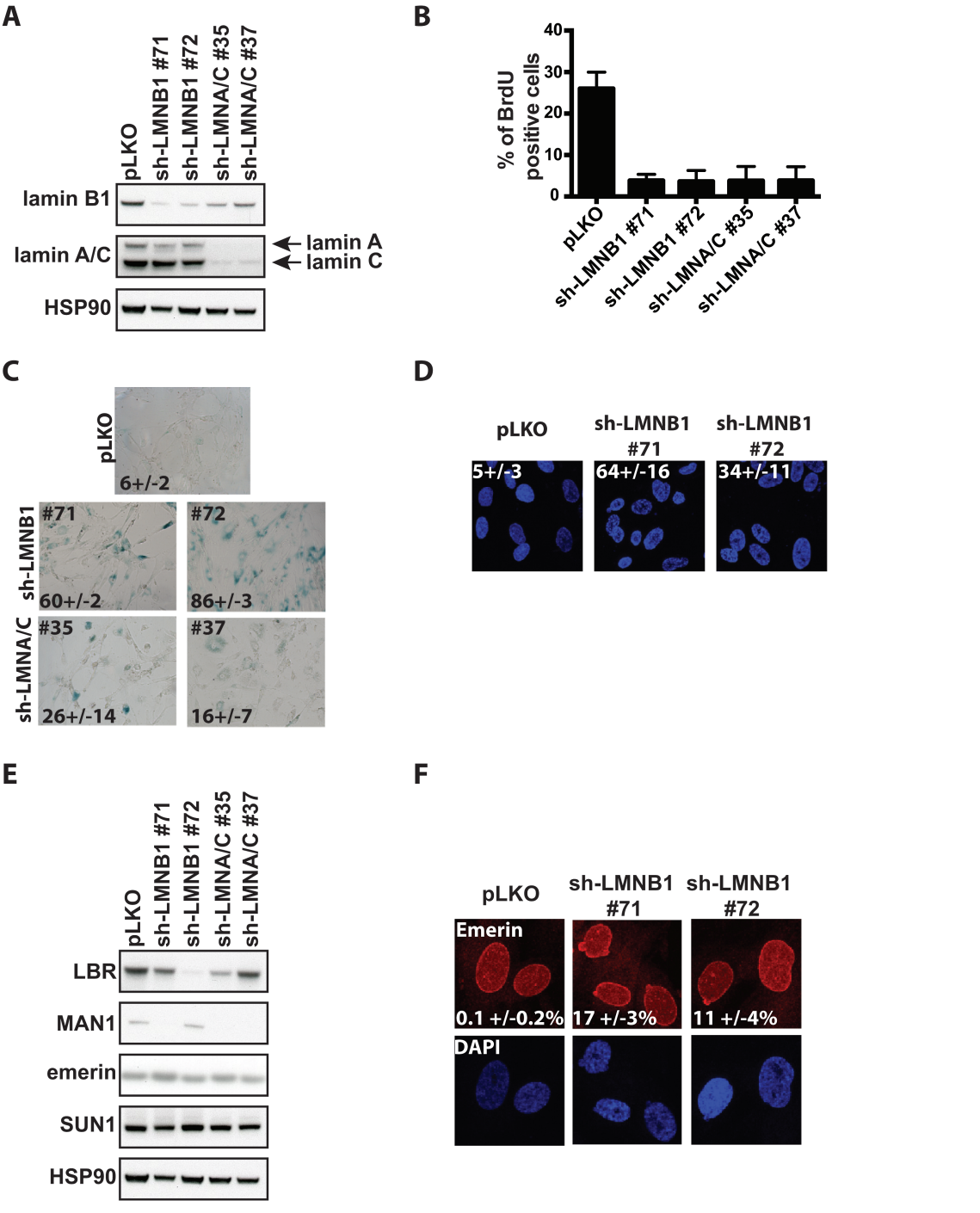

Figure 4. Depletion of lamin B1 or lamin A/C recapitulates partially the senescence phenotype and the NE defects seen in OIS cells. (**A**) Immunoblotting for lamin B1 and A/C of lysates from Tig3 fibroblasts harvested 8 days after transduction with the indicated shRNAs. (**B**) BrdU incorporation analysis of Tig3ET cells performed 8 days after transduction with the indicated shRNAs. Data represent mean of three independent experiments. Error bars represent standard deviation. The differences between LMNB1 or LMNA/C shRNAs and pLKO were all statistically significant ($P < 0.05$ according to a two-tailed paired t-test) (**C**) SA-β-galactosidase staining of Tig3ET cells transduced with the indicated shRNAs. Numbers are the mean % of SA-β-galactosidase positive cells (mean and confidence interval from three independent experiments). The differences between LMNB1 shRNAs and pLKO are statistically significant ($P < 0.001$ for sh-LMNB1 #71 and $P < 0.01$ for sh-LMNB1 #72, according to a two-tailed paired t-test). (**D**) DAPI staining of cells shown in (A), (B), (C). Numbers are % of cells showing SAHF accumulation. Data are based on three independent experiments and are presented as mean +/- confidence interval ($n = 200$). The difference between sh-LMNB1 #71 and pLKO is statistically significant ($P < 0.05$ according to a two-tailed paired t-test). (**E**) Immunoblotting analysis of lamin and INM proteins after LMNB1 or LMNA/C knockdown. Tig3ET transduced with either *LMNB1* or *LMNA/C* shRNAs were harvested and lysed 8 days after lentiviral transduction. (**F**) Confocal immunofluorescence microscopy for emerin in LMNB1 knockdown Tig3ET cells. Numbers are % of cells with nuclear blebs. Data are based on three independent experiments and are presented as mean ± confidence interval ($n = 200$). The differences between LMNB1 shRNAs and pLKO are statistically significant ($P < 0.01$ for sh-LMNB1 #71 and $P < 0.05$ for sh-LMNB1 #72, according to a two-tailed paired t-test).

reported to be repressed in fibroblasts from Hutchinson–Gilford Progeria Syndrome (HGPS) patients (29). In addition, cells undergoing replicative senescence and tissues of aged individuals accumulate progerin (21). This led us to ask whether progerin expression was induced during OIS. For this, we performed qRT-PCR with primers specific for 150 *LMNA*, the transcript encoding

progerin. The levels of 150 *LMNA* mRNA were not significantly induced in $BRAF^{V600E}$ or $H\text{-}RAS^{G12V}$-senescent cells, whereas its induction was evident in replicative senescent cells and in human fibroblasts engineered to express exogenous GFP progerin (Supplementary Figure 5A, available at *Carcinogenesis* Online). We also performed immunofluorescent confocal microscopy using a progerin-specific antibody. Whereas this antibody readily detected progerin in cells expressing exogenous GFP progerin, as demonstrated by a nuclear signal colocalizing with GFP, it failed to detect any expression in OIS cells (Supplementary Figure 5B, available at *Carcinogenesis* Online). Therefore, progerin is unlikely to play a role in OIS-associated lamin downregulation.

We then asked whether the decreased levels of lamins and NE proteins were the result of transcriptional repression. QRT-PCR analysis did not detect any significant decrease in the levels of *LMNA/C*, *LMNB1* and *EMD* mRNA in OIS cells (Supplementary Figure 5C, available at *Carcinogenesis* Online), arguing against a regulation at the transcriptional level. In contrast, we observed a significant downregulation of *LMNB1* and *LBR* mRNAs in cells undergoing replicative senescence, indicating that transcriptional repression contributes to downregulation of these NE proteins in this senescence context (Supplementary Figure 5D, available at *Carcinogenesis* Online).

To investigate a role for increased protein degradation, we assessed the effect of protease inhibitors on the expression of lamins and of several INM proteins in OIS cells. Remarkably, both in the context of $BRAF^{V600E}$ and $H\text{-}RAS^{G12V}$-induced senescence, the expression levels of all NE proteins examined were restored by bafilomycin, an inhibitor of lysosomal V-ATPase but not by epoxomicin, a proteasome-specific inhibitor (Figure 5A and B and Supplementary Figure 5E and 5F, available at *Carcinogenesis* Online). A similar restoration was obtained using another lysosomal inhibitor, chloroquine (Figure 5C and D). Therefore, the downregulation of NE proteins during OIS is achieved by lysosomal proteolysis.

Lysosomal degradation represents the ultimate step of autophagy, prompting us to investigate a role for this process. Among the different types of autophagy, chaperone-mediated autophagy was unlikely to play a role as none of the NE proteins investigated contain the KFERQ-like pentapeptide—a recognition motif for the chaperon protein HSP70. Therefore, we turned our attention to macroautophagy. We investigated the effects of knocking down *ATG5*, a gene required for autophagosome formation, which is an essential step in this process. For this, we generated polyclonal Tig3ET cell lines expressing one of two independent non-overlapping *ATG5* shRNAs and then transduced these cells with $BRAF^{V600E}$-encoding lentivirus. Immunoblotting for ATG5 confirmed efficient knockdown by the two shRNAs and revealed upregulation of ATG5 in $BRAF^{V600E}$-senescent cells, indicative of autophagy induction (Figure 5E, also see below). Silencing of ATG5 markedly attenuated the OIS-induced downregulation of lamin B1, emerin, LBR and SUN1 in OIS cells (Figure 5E and F). However, the levels of lamin A and MAN1 were not restored. This could result from the combined effects of an incomplete block of autophagy conferred by *ATG5* shRNAs and an increased sensitivity of lamin A and MAN1 to autophagic degradation (see below). Nonetheless, these results implicate macroautophagy as an important contributor to the loss of NE protein expression during OIS.

OIS cells activate autophagy and lysosomal biogenesis

Enhanced degradation of NE proteins could be facilitated by autophagy activation. Therefore, we set out to determine whether our observations could be correlated with increased autophagy in $BRAF^{V600E}$-senescent cells. Consistent with previous work in $H\text{-}RAS^{G12V}$- and therapy-induced senescent cells (8–10), we could detect signs of autophagy activation during $BRAF^{V600E}$-induced senescence, such as conversion of LC3-I into its lipidated form LC3-II (Figure 6A). This induction of LC3 II was partially abrogated in cells that bypassed $BRAF^{V600E}$-induced senescence after ectopic SV40 st expression (Figure 6A and Supplementary Figure 6A, available at *Carcinogenesis* Online). $BRAF^{V600E}$-senescent cells also displayed an increase in the mRNA levels of the autophagy genes *ATG5, ATG7, ULK1* and the related gene *ULK3* (Supplementary Figure 6B, available at *Carcinogenesis* Online).

Along with autophagy activation, we observed several indicators of increased lysosomal activity. First, we detected an increase in the immunofluorescence signal for the lysosomal marker LAMP2 in $BRAF^{V600E}$-senescent cells, indicating an expansion of the lysosomal compartment. This phenotype was reversed upon SV40st-mediated OIS bypass (Figure 6B). In addition, the expression of the mature forms of several lysosomal proteases, including cathepsin C, D and L, and of lysosomal pro-X carboxypeptidase (PRPC) was induced in $BRAF^{V600E}$-senescent cells. This induction was markedly attenuated in cells bypassing OIS (Figure 6C). Mature forms of cathepsin D and cathepsin L also accumulated in $BRAF^{V600E}$-senescent IMR90ET and melanocytes (Supplementary Figure 6C, available at *Carcinogenesis* Online).

We then determined whether the differential regulation of lysosomal proteins occurs at the transcriptional level. In a gene expression data set previously generated in our lab (30), we found that several genes encoding lysosomal proteases were induced in $BRAF^{V600E}$-senescent cells in comparison to proliferative or cells bypassing OIS by depletion of C/EPB (Supplementary Figure 6D, available at *Carcinogenesis* Online). These genes included *CTSB, CTSD, CTSL, CTSO, CTSS, DPP4* and *DPP7*. The upregulation of these lysosomal genes in OIS cells was confirmed by RT-qPCR (Figure 6D). Overall, these data show that transcriptional regulation contributes to the activation of the autophagy program during OIS.

To further explore the relationship between NE protein repression and autophagy activation, we performed a time course to determine the kinetics of NE protein expression and autophagy/lysosomal activity regulation following exposure to $BRAF^{V600E}$-encoding retroviruses. In this experiment, senescence occurred within 4 days after retroviral transduction, as manifested by a decrease in BrdU incorporation and an induction of p16 (Figure 6E and F). Increase in ATG5 expression and induction of mature forms of cathepsin D and L were apparent at day 4, correlating with the timing of induction of senescence. The downregulation of NE proteins also began at day 4, albeit with varying kinetics. While lamin A and MAN1 already showed a marked decrease at day 4, a clear downregulation of lamin B1, LBR, emerin and SUN1 was only evident at day 6 post-$BRAF^{V600E}$ introduction, indicating that lamin A and MAN1 are more sensitive to autophagic degradation than the other NE proteins (Figure 6F). In any case, the finding that NE protein downregulation occurs concomitantly or after the activation of cathepsins reinforce the idea that the lysosomal peptidases are responsible for NE protein degradation during OIS. This is further supported by the observation that Bafilomycin could largely prevent the formation of mature cathepsin C, D and PRPC in OIS cells (Supplementary Figure 6E, available at *Carcinogenesis* Online).

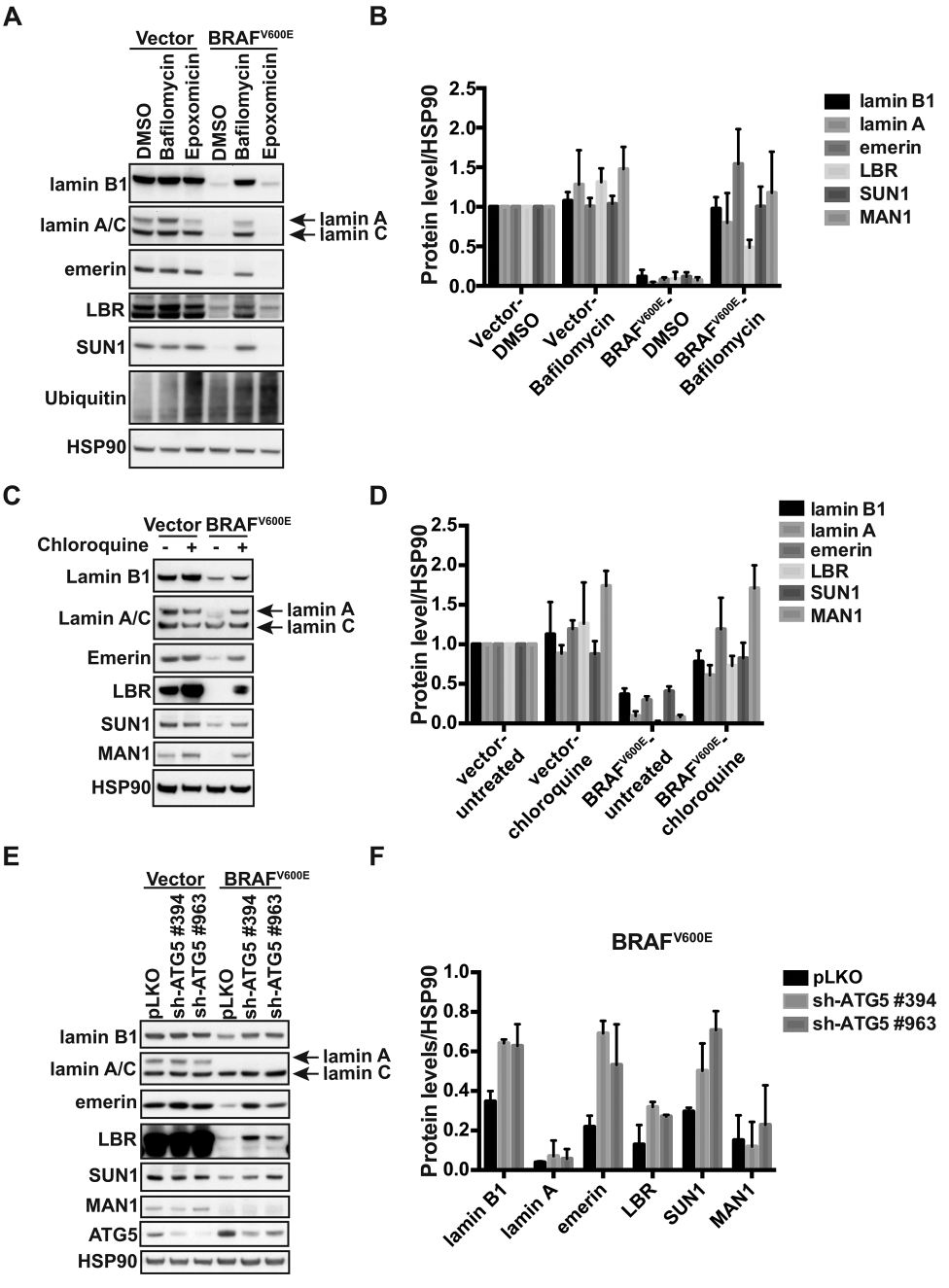

Figure 5. Downregulation of NE proteins upon OIS is caused by autophagy. (**A**) Immunoblotting showing that bafilomycin A1 but not epoxomicin restores NE protein levels in OIS. Seven days after BRAF^{V600E} retroviral transduction, cells were treated with 100 nm bafilomycin for 8 h or with 1mM epoxomicin for 4 h before harvesting. The accumulation of ubiquitinated proteins indicates efficient proteasome inhibition by epoxomicin. (**B**) Quantification of the WB signal from (A). Protein levels were normalized to HSP90. Data are presented as mean and standard deviation of three independent experiments. The differences between BRAF^{V600E}-DMSO and BRAF^{V600E}-bafylomycin were statistically significant for all the proteins examined with $P < 0.05$ in all cases according to a two-tailed paired *t* test. (**C**) Immunoblotting showing the restoration of NE proteins levels in OIS by chloroquine treatment. Cells were treated with 100 M chloroquine for 6 h before harvesting. (**D**) Quantification of the WB signal from (C). Protein levels were normalized to HSP90. Data are presented as mean and standard deviation of three independent experiments. The differences between BRAF^{V600E}-DMSO and BRAF^{V600E}-chloroquine were statistically significant with $P < 0.05$ in all cases but lamin B1 according to a two-tailed paired *t* test. (**E**) Immunoblotting of Tig3ET cells transduced with empty vector or sh-ATG5 shRNAs lentiviruses and subsequently infected with BRAF^{V600E} -encoding lentiviruses. Cells were harvested 8 days after BRAF^{V600E} lentivirus infection. (**F**) Quantification of the WB signal from (E). Protein levels were normalized to HSP90. Data are presented as mean and standard deviation of two independent experiments.

Discussion

In this study, we show that OIS is associated with loss of lamins B1 and A, as well as several INM proteins. Lamin B1 and, less consistently, lamin A, LBR and LAP2 have previously been shown to be downregulated during senescence (22–26). Our work confirms and extends these findings, by showing that OIS cells undergo an overall loss of NE proteins. Cells undergoing replicative senescence and senescence induced by a DNA damaging drug also display a decline in lamin levels, and some INM proteins. This indicates that NE protein depletion is a common

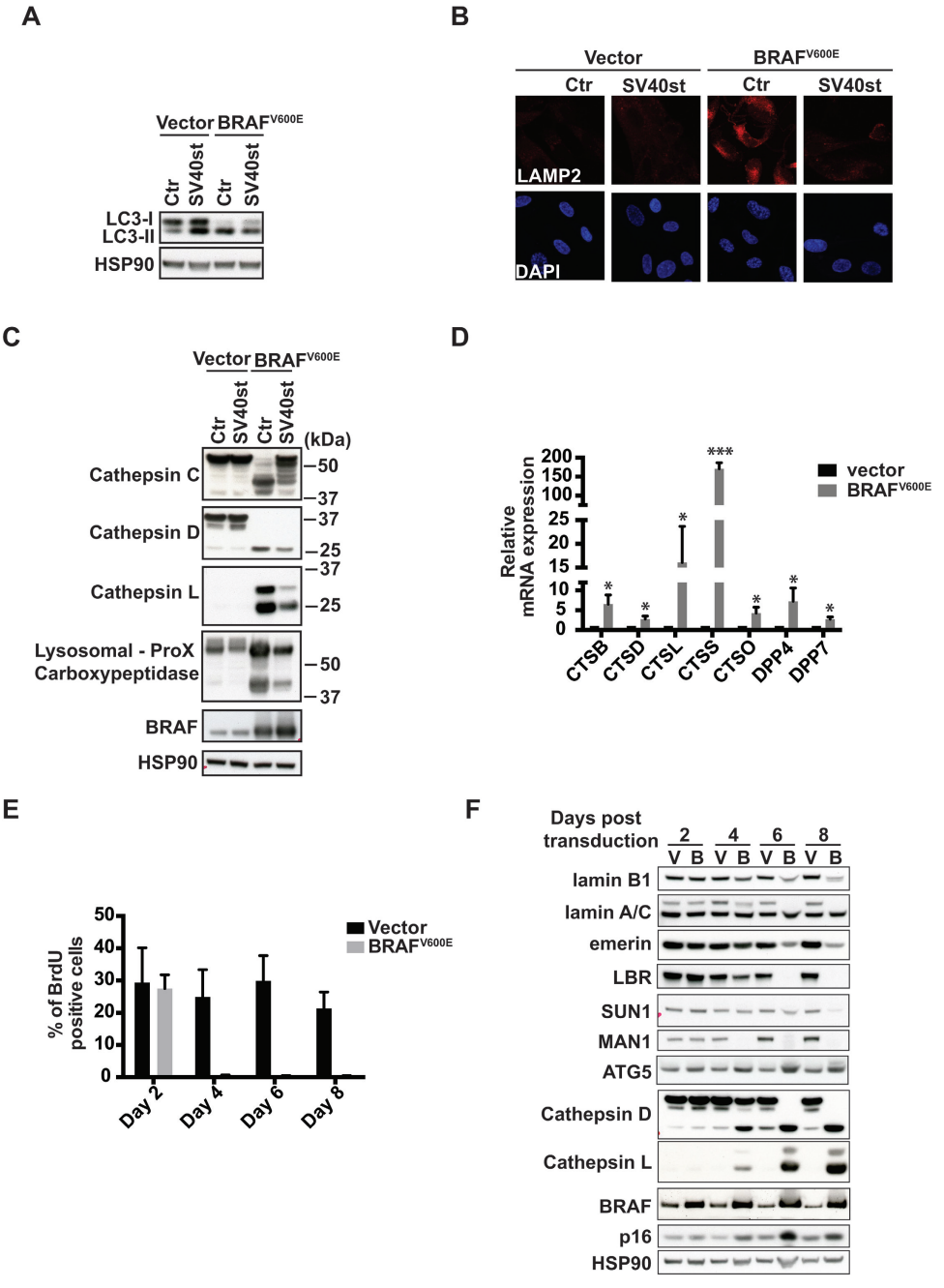

Figure 6. BRAF^{V600E}-senescent cells display increased autophagy and lysosomal activity. (**A**) Immunoblotting for LC3 from lysates from Tig3ET fibroblasts transduced with the indicated retroviruses. (**B**) Immunofluorescence confocal microscopy for LAMP2 in cells infected with the indicated constructs. DAPI was used for DNA staining. (**C**) Immunoblotting of lysates from Tig3ET fibroblasts harvested 7 days after transduction with empty vector or BRAF^{V600E} retroviruses with antibodies against the indicated lysosomal peptidases. Results in A–C are representative of at least three independent experiments. (**D**) qRT-PCR analysis for lysosomal genes of mRNA derived from Tig3ET cells infected with the indicated constructs. Data are normalized to control vector cells and presented as mean and standard deviation of three independents experiments. Asterisks indicate $P < 0.05$ (*), $P < 0.001$ (***), based on a two-tailed paired *t* test. (**E**) BrdU incorporation analysis of Tig3ET cells transduced with empty vector or BRAF^{V600E} at the various indicated time points after retroviral transduction. Data are presented as mean and standard deviation of two independent experiments. (**F**) Immunoblotting from lysates from cells shown in (E). V = empty vector, B = BRAF^{V600E}. Results shown are representative for two independents experiments.

characteristic of senescence that could be used as a biomarker thereof.

We also found OIS and replicative senescence to be associated with NE shape alterations. Consistent with our observations, NE deformation was previously reported to occur in replicatively senescent human mesenchymal stem cells (31); however, how these morphological changes arise during OIS was unknown. While individual depletion of lamin B1 and lamin A/C is not sufficient to reproduce the OIS-associated NE deformation, it is likely that the overall depletion of the NE constituents results in the destabilization of the NE structure. Nuclear shape alterations were also reported in the context of Ras-induced senescence and IR-induced senescence, although in this study senescence was associated with lamin B1 upregulation rather than downregulation (32). While the reason for the discrepancy in lamin B1 levels is unclear, these findings suggest that

the levels of lamins, and possibly other NE proteins too, must be tightly regulated in order to maintain a proper NE structure.

Individual depletion of lamins B1 and A/C recapitulated partially the senescence features and NE defects seen in OIS, suggesting that their repression may actively participate in the OIS-associated NE changes and senescence process.

Alterations of NE composition and structure are likely to have deleterious effects on its functions, particularly with respect to its role as a physical barrier between the nuclear and cytoplasmic compartments. Indeed, a previous study has reported that senescent cells show increased NE permeability associated with an aberrant localization of chromatin fragments in the cytoplasm (25). Another possible consequence of the observed NE alterations is the perturbation of genome–NL interactions (16) and resulting alteration of tridimensional chromatin organization in the nucleus. Accordingly, widespread changes in lamin B1 interactions with the genome have been reported during H-RAS^{G12V}-induced senescence (33).

In contrast to what we and others observed in replicative or irradiation-induced senescence (22–24), we failed to detect any reproducible decrease of lamin B1 mRNA in OIS cells. Therefore, while transcriptional repression may contribute to lamin B1 repression in these other types of senescence, it does not appear to represent a major mechanism of downregulation in the context of OIS.

We found that depletion of lamins and INM proteins was prevented by inhibition of autophagy, implicating this process as the mechanism responsible for their degradation. How the NE proteins are targeted to the autophagy machinery during OIS remains to be determined. One possibility is that ROS accumulation that typically accompanies OIS (7,34) can result in irreversible lesions of NE proteins. Alternatively, chromosome condensation resulting in SAHF formation (35) or lamin phosphorylation due to enhanced MAPK signaling could be perceived as a signal for NE breakdown (36). These two scenarios could result in the dissociation of lamins and INM proteins from the nuclear membrane and their diffusion in the cytoplasm where they become accessible for degradation by the autophagic machinery. Of note, the NE proteins may not be the only nuclear substrates for degradation by the autophagy pathway during OIS, as histone H3 has also been reported to be cleaved by lysosome-mediated proteolysis (25). Whether this phenomenon is specific to NE proteins and histones or whether it affects nuclear proteins more generally remains to be determined. Notably, autophagic degradation of nuclear components can also occur in biological contexts other than senescence. Indeed, autophagosomes containing chromatin have been described in human and mouse cells lacking lamin A or emerin (37) and in human cells treated with cell cycle inhibitors (38).

We found that similarly to H-RAS^{G12V} and therapy-induced senescence (8–10), cells undergoing senescence following exposure to the oncogene BRAF^{V600E}, displayed elevated autophagy and lysosomal activity which coincided with the onset of NE protein loss. In particular, we found that several lysosomal proteases are upregulated in OIS cells, some of which were not previously associated with senescence. Their specific role in the cleavage of the NE proteins and in the implementation of senescence remains a subject for further study. In any case, their upregulation provides novel biomarkers for the monitoring OIS. Of note, the induction of autophagy and lysosomal genes in BRAF^{V600E}-senescent cells occurred at the transcriptional level. Further work will be necessary to identify the transcription factor(s) responsible for the activation of the autophagy program during OIS.

In conclusion, we found that lamins and INM proteins undergo autophagic degradation during OIS. We have thus identified an unexpected connection between NE alterations—a change affecting the nucleus—and enhanced degradative processes occurring in the cytoplasmic compartment.

Supplementary material

Supplementary Figures 1–6 and Table 1 can be found at http://carcin.oxfordjournals.org/

Funding

The Netherlands Organization for Scientific Research (NWO-ALW, Project number: 822.02.001)

Acknowledgements

We thank Anita Pfauth and Frank van Diepen in assisting with flow cytometry, Lenny Brocks and Lauran Oomen for technical assistance in using the microscopy facility, Hans Janssen for electron microscopy imaging. We thank Nathalie Moatti for English editing of the manuscript.
Conflict of Interest Statement: None declared.

References

1. Kuilman, T. et al. (2010) The essence of senescence. Genes Dev., 24, 2463–2479.
2. Michaloglou, C. et al. (2005) BRAFE600-associated senescence-like cell cycle arrest of human naevi. Nature, 436, 720–724.
3. Collado, M. et al. (2005) Tumour biology: senescence in premalignant tumours. Nature, 436, 642.
4. Braig, M. et al. (2005) Oncogene-induced senescence as an initial barrier in lymphoma development. Nature, 436, 660–665.
5. Chen, Z. et al. (2005) Crucial role of p53-dependent cellular senescence in suppression of Pten-deficient tumorigenesis. Nature, 436, 725–730.
6. Dankort, D. et al. (2009) Braf(V600E) cooperates with Pten loss to induce metastatic melanoma. Nat. Genet., 41, 544–552.
7. Kaplon, J. et al. (2013) A key role for mitochondrial gatekeeper pyruvate dehydrogenase in oncogene-induced senescence. Nature, 498, 109–112.
8. Dörr, J.R. et al. (2013) Synthetic lethal metabolic targeting of cellular senescence in cancer therapy. Nature, 501, 421–425.
9. Young, A.R. et al. (2009) Autophagy mediates the mitotic senescence transition. Genes Dev., 23, 798–803.
10. Narita, M. et al. (2011) Spatial coupling of mTOR and autophagy augments secretory phenotypes. Science, 332, 966–970.
11. Narita, M. et al. (2003) Rb-mediated heterochromatin formation and silencing of E2F target genes during cellular senescence. Cell, 113, 703–716.
12. Zhang, R. et al. (2007) Molecular dissection of formation of senescence-associated heterochromatin foci. Mol. Cell. Biol., 27, 2343–2358.
13. Burke, B. et al. (2013) The nuclear lamins: flexibility in function. Nat. Rev. Mol. Cell Biol., 14, 13–24.
14. Dechat, T. et al. (2010) Nuclear lamins. Cold Spring Harb. Perspect. Biol., 2, a000547–a000547.
15. Amendola, M. et al. (2014) Mechanisms and dynamics of nuclear lamina-genome interactions. Curr. Opin. Cell Biol., 28, 61–68.
16. Guelen, L. et al. (2008) Domain organization of human chromosomes revealed by mapping of nuclear lamina interactions. Nature, 453, 948–951.
17. Peric-Hupkes, D. et al. (2010) Role of the nuclear lamina in genome organization and gene expression. Cold Spring Harb. Symp. Quant. Biol., 75, 517–524.
18. Eriksson, M. et al. (2003) Recurrent de novo point mutations in lamin A cause Hutchinson-Gilford progeria syndrome. Nature, 423, 293–298.
19. De Sandre-Giovannoli, A. et al. (2003) Lamin a truncation in Hutchinson-Gilford progeria. Science, 300, 2055.
20. McClintock, D. et al. (2006) Hutchinson-Gilford progeria mutant lamin A primarily targets human vascular cells as detected by an anti-Lamin A G608G antibody. Proc. Natl. Acad. Sci. USA, 103, 2154–2159.

21. Scaffidi, P. et al. (2006) Lamin A-dependent nuclear defects in human aging. Science, 312, 1059–1063.
22. Shimi, T. et al. (2011) The role of nuclear lamin B1 in cell proliferation and senescence. Genes Dev., 25, 2579–2593.
23. Freund, A. et al. (2012) Lamin B1 loss is a senescence-associated biomarker. Mol. Biol. Cell, 23, 2066–2075.
24. Dreesen, O. et al. (2013) Lamin B1 fluctuations have differential effects on cellular proliferation and senescence. J. Cell Biol., 200, 605–617.
25. Ivanov, A. et al. (2013) Lysosome-mediated processing of chromatin in senescence. J. Cell Biol., 202, 129–143.
26. Shah, P.P. et al. (2013) Lamin B1 depletion in senescent cells triggers large-scale changes in gene expression and the chromatin landscape. Genes Dev., 27, 1787–1799.
27. Moiseeva, O. et al. (2011) Retinoblastoma-independent regulation of cell proliferation and senescence by the p53-p21 axis in lamin A/C-depleted cells. Aging Cell, 10, 789–797.
28. Shimi, T. et al. (2008) The A- and B-type nuclear lamin networks: microdomains involved in chromatin organization and transcription. Genes Dev., 22, 3409–3421.
29. Scaffidi, P. et al. (2005) Reversal of the cellular phenotype in the premature aging disease Hutchinson-Gilford progeria syndrome. Nat. Med., 11, 440–445.
30. Kuilman, T. et al. (2008) Oncogene-induced senescence relayed by an interleukin-dependent inflammatory network. Cell, 133, 1019–1031.
31. Raz, V. et al. (2008) The nuclear lamina promotes telomere aggregation and centromere peripheral localization during senescence of human mesenchymal stem cells. J. Cell Sci., 121, 4018–4028.
32. Barascu, A. et al. (2012) Oxidative stress induces an ATM-independent senescence pathway through p38 MAPK-mediated lamin B1 accumulation. EMBO J., 31, 1080–1094.
33. Sadaie, M. et al. (2013) Redistribution of the Lamin B1 genomic binding profile affects rearrangement of heterochromatic domains and SAHF formation during senescence. Genes Dev., 27, 1800–1808.
34. Ogrunc, M. et al. (2014) Oncogene-induced reactive oxygen species fuel hyperproliferation and DNA damage response activation. Cell Death Differ., 21, 998–1012.
35. Narita, M. et al. (2003) Rb-mediated heterochromatin formation and silencing of E2F target genesduring cellular senescence. Cell, 113, 703–716.
36. Margalit, A. et al. (2005) Breaking and making of the nuclear envelope. J. Cell. Biochem., 95, 454–465.
37. Park, Y.E. et al. (2009) Autophagic degradation of nuclear components in mammalian cells. Autophagy, 5, 795–804.
38. Rello-Varona, S. et al. (2012) Autophagic removal of micronuclei. Cell Cycle, 11, 170–176.